Investigation into modelling and improving an axial flux, permanent magnet synchronous motor for a solar race car.

Abstract – This paper models and analyses the flux gap and losses found in the axial flux permanent magnet motor used in the Durham University Solar Car (DUSC), pictured below in Figure 1. A Halbach array, as well as pole number, are investigated to try to optimise the design without affecting the current stator. Finally, new, sinusoidally sculpted back irons are designed and manufactured that save over 3kg from the previous edition of rotor.

Index terms – Topic - Axial Flux, Halbach Array, Eddy Currents, Winding Factor, Flux Saturation, Solar Power, Electric Vehicles.

Figure 1: The Durham University Solar Car 2019

I. Introduction

In this report, an analysis of the current Durham University Solar Car motor is carried out. Beginning with modelling the machine in Excel and MatLab, and then moving to full 3D FEA. Then, the magnetic topology of the rotor will be studied, and optimisations made. The stator will not be investigated in this report, as such the rotor will be designed to be the best possible match to the current 12 coil stator

Within this work alterations to the magnetic topology of the machine, namely pole number, a Halbach array, and sculpted back irons are investigated to try and improve the DUSC motor, '*Eadfrith*'. Simultaneously, simulations are run to better classify the losses and efficiency of the machine and compare it to an analytical model.

II. Machine Design

An excel spreadsheet was designed to generate machine parameters based on specified inputs for axial flux permanent magnet machines with non-overlap windings. Figure 1 shows an example stator from one of the current solar car motors, *Eadfrith*.

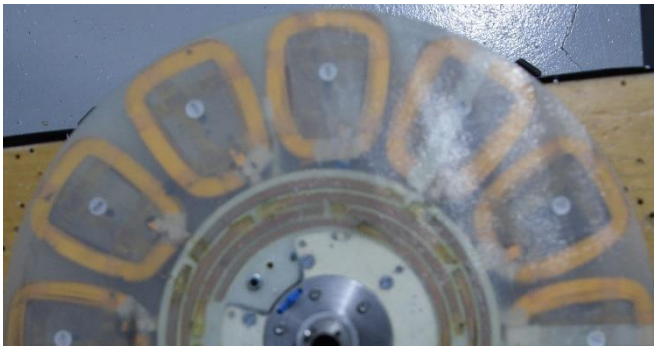

Figure 2: 12 Coil Stator from Eadfrith

The spreadsheet generates valuable information such as power consumed, torque developed, and efficiency. Table 1 shows some of the required input parameters and values used for comparison with the FEA model.

Table 1: Sample input parameters

Speed (RPM)	657
Number of poles	16
Number of coils	12
Running clearance (mm)	2
Stator thickness (mm)	8
Magnet radial length (mm)	69
Magnet thickness (mm)	6
Wheel Circumference (m)	1.65
Saturation flux density (T)	1.6

Magnet 3D was used to simulate the same machine to compare the results obtained from calculations with those obtained from finite element analysis.

A. Flux Gap Modelling

The air gap was modelled based on the method used in [1]. By modelling a current sheet on the edge of the magnets with a sinusoidal waveform circumferentially about the machine, the flux in the air gap could be modelled with equation

$$B_{yn}(x) = \frac{J_n u_0}{u_n} \frac{\sinh(u_n t_m)}{\sinh(u_n \frac{g}{2})} \cos(u_n x) \qquad (1)$$

Where n is the harmonic number, t_m is the thickness of the magnets, g is the distance between rotor discs, and J_n is the equivalent current density given by

$$J_n = \frac{4}{\tau}\frac{B_r}{u_0 u_{rec}}\sin\left(\frac{u_n d_m}{2}\right) \quad (2)$$

Where τ is the pole pitch, d_m is the magnet width, and $u_n = \frac{\pi n}{\tau}$.

MagNet 3D was used to model the same machine and field arc probe used to obtain the flux halfway across the air gap. Figure 3 shows both the flux obtained from the method outlined above, and that found from FEA.

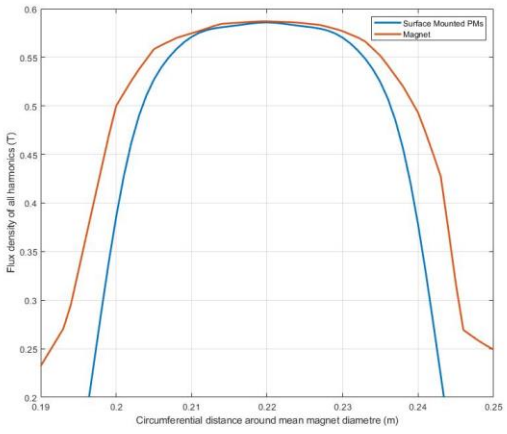

Figure 3: Flux Density in the air gap

The FEA clearly backs up the analytical model, with the peak value of flux being 0.586T and 0.5872T for the analytical and FEA model respectively. The larger spread observed in the MagNet model is likely due fringing flux in-between the poles that is not accounted for in the analytical model.

Given that the FEA backs up the spreadsheet model to within 0.2%, it can be used to model the flux in the air gap for the machine reliably.

B. Electrical Losses

The machine being designed is a coreless machine, thus there are no eddy current or hysteresis core losses in the stator. This means the only electrical losses should come from ohmic losses and eddy currents in the stator windings. The ohmic losses per coil can be calculated quite easily by

$$P_{ohmic} = I^2 R \quad (3)$$

Where I is the armature current, and R is the resistance of the coil calculated by

$$R = \frac{\rho L}{A} \quad (4)$$

Where ρ is the resistivity of copper at the operating temperature, L is the total length of wire in the coil (mean turn length x number of turns), and A is the cross-sectional area of the copper strip.

Eddy losses are created with the motion of the PMs relative to the stationary stator winding, producing an alternating field through the conductors and thus inducing eddy currents. To calculate the eddy current losses the equation

$$P_{eddy} = \frac{\pi^2}{3}\frac{\sigma}{\rho} f^2 a^2 m_{con}[B_{mx1}^2 + B_{mz1}^2]\eta_n^2 \quad (5)$$

is used [2]. Where σ and ρ are the electrical conductivity and specific mass density of the copper respectively, f is the stator current frequency, a is the width of the conductor (parallel to the stator plane), m_{con} is the mass of the conductors, B_{mx1} and B_{mz1} are the peak values of tangential and axial components of the magnetic flux density, and η_n is the coefficient of distortion – assumed to be 1 for sinusoidal distribution of flux.

Magnet 3D was used to construct the entire machine to simulate a moving machine and verify losses. Using SolarSim4, a program used by Durham University Electric Motorsport, and the input parameters for the 2019 car, a target cruise speed of roughly 65kph was obtained for the 3000km race.

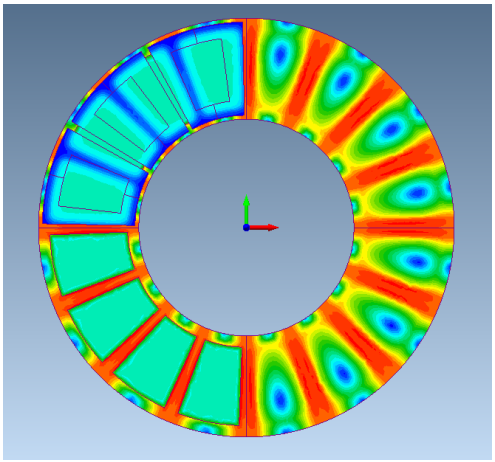

Figure 4: Magnet model showing flux in back-iron and through 3 coils

The torque required to maintain the car at this speed can be calculated by

$$T = \frac{D}{2}\left(\frac{1}{2}\rho v^2 C_{DA} + \mu_r M g\right) \quad (6)$$

Where D is the diameter of the motor wheel, ρ is the density of air, v the vehicle velocity, C_{DA} the coefficient of drag for the solar car, μ_r the rolling resistance, M the total mass of car and driver, and g is acceleration due to gravity.

For the desired cruising speed of 65kph, a total of 12.5N of torque is required to be developed by the

machine. According to the spreadsheet, an armature current of 7.5A is needed to generate this torque at a frequency of 87.65Hz. This was supplied to the coils in MagNet, and a load torque of 12.5N was applied to the machine to compare Back EMF voltages induced and losses between the spreadsheet and the FEA model. Table 2 shows some of the different values between the two machines.

Table 2: Analytical and Finite Element comparison

	Spreadsheet	MagNet 3D
Phase Voltage (V)	38.159	35.566
Machine Power (W)	858.929	822.273
Efficiency (%)	95.339	93.550

As can be seen above, there is a noticeable difference between the values calculated by the spreadsheet and those obtained using finite element analysis. The MagNet model generated much lower back EMFs to run at this speed, therefore reducing the required machine power. Efficiency was also lower for the FEA model, likely due to its better ability to quantify losses.

Unfortunately, experimental tests will have to be carried out to verify which of these models is more reliable – for now the spreadsheet model will be carried forward.

C. Machine Verification

For further analysis with experimental data, measurements of the static torque at different phase angles was obtained from FEA, as well as the relationship between Back EMF and increasing speed.

Figures 5 and 6 show the static torque against phase angle and back emfs with increasing speed respectively.

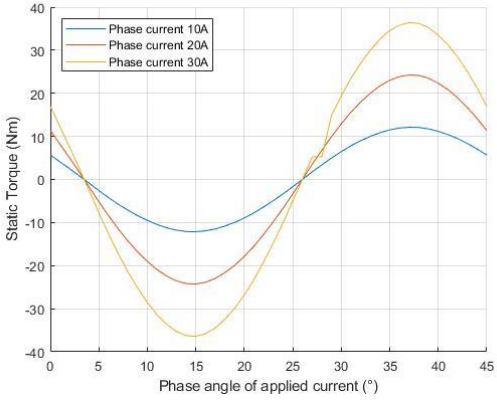

Figure 5: Static Torque Measurements

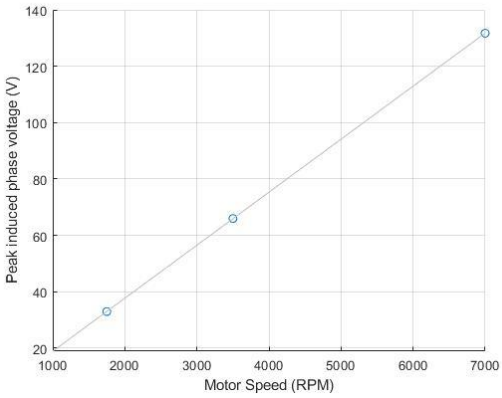

Figure 6: Induced EMF measurements

III. Rotor Improvements

A. Halbach Array

A Halbach array is where the magnetisation vector of the permanent magnets rotates as a function of their distance along the array as shown in Figure 7.

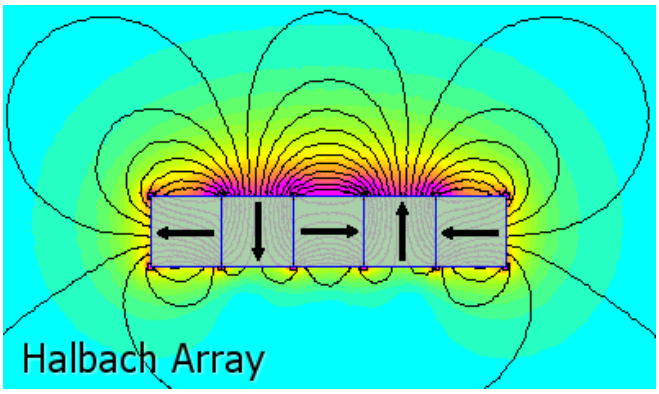

Figure 7: Linear Halbach array

This type of array has multiple advantages over the standard steel backing plate outlined previously as it can increase the strength of the fundamental field by a factor of 1.4. Also, with the flux being directed through the magnets there is no need for a steel backing plate, and so a lot of weight can be saved. Finally, the more magnets used to direct the flux the more uniformly sinusoidal the flux in the air gap.

The strength of the magnetic field for a double sided axial Halbach array can be calculated using

$$B_z(x,z) = B_{m0}\sin(\beta x)\frac{1}{\cosh(\frac{\beta t}{2})}\cosh(\beta z) \qquad (7)$$

Where beta is $\beta = \frac{2\pi}{l_a}$, l_a is the spatial period or wavelength of the array, and B_{m0} is the peak value of the magnetic flux density at the active surface of the Halbach array given by

$$B_{m0} = B_r[1-\exp(-\beta h_M)]\frac{\sin(\frac{\pi}{n_M})}{\frac{\pi}{n_M}} \qquad (8)$$

Where B_r is the remnant flux density of the magnets, h_M is the height of the magnets, and n_M is the number of PMs per wavelength.

From these equations, there are three factors that contribute to a powerful Halbach array – A larger number of magnets per wavelength, the shortest possible wavelength, and the thickest possible magnets.

A 16 pole Halbach array was generated using these formula and the current machine parameters, i.e. $h_M = 6$, and $l_a = 110$mm. The resulting axial flux in the air gap is shown in Figure 8 using 4 magnets per wavelength.

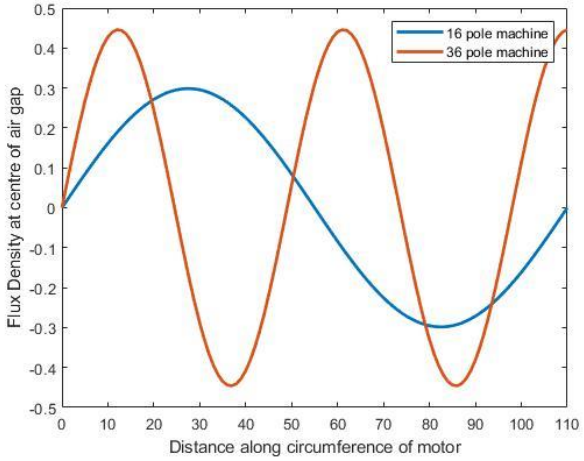

Figure 8:Comparison of a 16-pole and 36-pole Halbach array

As can be seen, the peak flux density is much lower than when using a conventional array and is due to the large wavelength imposed on the array by the size of the machine.

A 36-pole machine, like the one designed in [3] was modelled to compare the flux in the air gap with a resulting wavelength of 49mm. As can be seen in Figure 6, a higher peak flux density was achieved. The machine designed in [3] used N40 grade magnets and was able to achieve a peak flux density of 0.758T at the centre of the air gap.

A Halbach array was not pursued for development of the DUSC motor as increasing the number of poles to the extent needed to benefit from a Halbach array would require redesigning the stator to employ overlapping windings much like the 40-pole CSIRO motor [4].

B. Number of Poles

The affect of changing the number of poles was then investigated, like how an 18-coil stator was investigated in [5]. The relationship between the number of poles and the number of coils is represented by the winding factor given by

$$K_w = K_p K_d \tag{9}$$

with the pitch factor K_p being the ratio of phasor sum to arithmetic sum of the EMFs per coil side, and the distribution factor K_d being the ratio between the phasor sum to arithmetic sum of EMFs induced per coil.

$$K_p = \frac{\sin\left(\frac{\pi}{2m}\right)}{z\sin\left(\frac{\pi}{2mz}\right)} \tag{10}$$

was used to obtain the pitch factor. Where $z = \frac{Q_c}{mF}$, Q_c is the number of stator slots, m the number of phases, and F the number of pole sections given by F= GCD(2p,Q_c), where p is the number of pole pairs.

The pitch factor was calculated using

$$K_p = \sin\left(\frac{\theta_m - \theta_{re}}{2}\right)\frac{\sin\left(\frac{\theta_{re}}{2}\right)}{\frac{\theta_{re}}{2}} \tag{11}$$

where θ_{re} is the electrical angle corresponding to the coil layer width, and $\theta_m = \frac{2\pi p}{Q_c}$.

Figure 9 shows how the winding factor changes with the number of poles for a 12 coil stator, unsurprisingly a value of 0.994 is achieved at P = 12 where the coil pole pitch is perfectly matched to the magnet pole pitch, the only reason it's not unity is due to the packing factor of the coils.

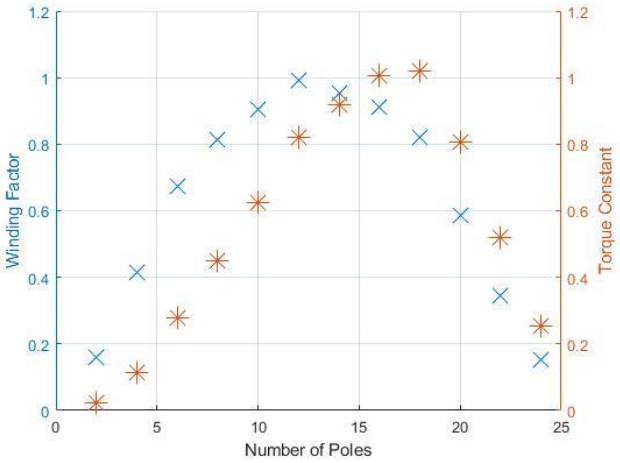

Figure 9: Winding Factors and Torque Constants

The winding factor has a direct affect on the torque constant of the machine, a useful parameter for classifying the quality of a motor. The torque constant for different pole variations was calculated using

$$K_T = \frac{m}{\sqrt{2}} pNK_w\Phi_f \quad (12)$$

Where N is the number of turns per coil, and Φ_f the flux in the air gap. The resulting torque constants are also plotted on Figure 7 where the best torque constant would be achieved from an 18-pole machine.

Whilst increasing the number of poles would increase the torque production by 10%, it was decided to stick to a 16-pole machine to avoid incurring the cost of new magnets.

C. Sculpted Back Irons

Iron makes a perfect material for back irons as it has practically zero reluctance, however this only remains the case for flux densities below about 1.6-1.8T depending on the type of steel [6]. Any higher flux density will only serve to increase the reluctance of the back iron, and thus cause a significant portion of the MMF to be used to drive the flux through the back iron.

Provided the saturation flux density remains below 1.6T, the proposal was to model two types of sculpted back irons – one that went straight from 2mm at the centre of each pole to 6mm at the extremities of the magnets, and another that had a sinusoidal waveform sculpted in line with the rate of flux flowing into the back iron from the air gap.

The minimum thickness required for the back iron to be was obtained using

$$t_i = \frac{\Phi_i}{2r_i B_i} \quad (13)$$

Where $\Phi_i = \frac{\Phi_t}{2}$ so half the total flux across the air gap, r_i is the radial length of the back iron, and B_i is the saturation flux density of the steel, taken to be 1.6T.

Using the parameters for Eadfrith, this gives a minimum of 6.3mm – much less than the current 8mm back irons. However, this assumes no leakage flux, and that the magnets haven't degraded and so 6mm back irons were pursued. Table X shows the weight and weight saved using 8mm flat, linearly sculpted, and sinusoidally sculpted back irons.

Table 3: Back-iron comparison weights

	Weight (kg)	Weight saved (kg)	Weight saved (%)
Flat 8mm	9.833	-	-
Flat 6mm	7.375	2.458	24.997
Linear 6mm	4.917	4.916	49.995
Sinusoidal 6mm	5.588	4.245	43.171

Opting for linearly sculpted, 6mm back irons would save the most weight. However, finite element analysis will be conducted to ensure that the flux density does not saturate in the back iron and that the flux in the air gap remains unchanged from the original back irons.

The machine was modelled in MagNet 3D to ensure that the flux density did not saturate. The linearly sculpted back irons were showing signs of saturation with flux at 1.7T at certain points and so sinusoidally sculpted back irons were carried forwards as the flux density did not exceed 1.6T.

The flux in the air gap was then measured for 8mm flat, and 6mm sinusoidal back irons and results plotted in figure 11.

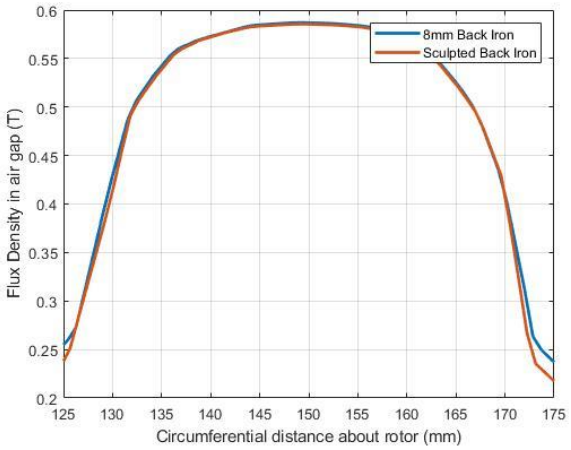

Figure 10: Comparison of sculpted back-iron to flat

As can be seen, there is no difference in the air gap flux density between the original 8mm back irons and the new 6mm sculpted back irons.

D. Finite Element Analysis

Given the unique shape of the back iron, rigorous FEA was performed to ensure that they would not fail when used in the solar car.

The parts were made in Solidworks and exported to Abaqus FEA where the worst possible loading condition for the wheel was simulated; a 4g bump, 1.5g brake, and 1g corner. Material properties of hardened steel were used with a young modulus of 215GPa and yield stress of 200MPa. Table 2 shows the resulting stresses and factors of safety from the analysis.

	LHS Back Iron	RHS Back Iron
Max Displacement (mm)	0.2158	0.1854
Peak VM Stress (MPa)	50	40
Factor of Safety	4	5

The analysis shows that both back irons are more than suitable for use in the solar car, with the left-hand side back iron having a factor of safety of 4, and the right-hand side back iron having a factor of safety of 5.

IV. Conclusions

In conclusion, the comparison between analytical methods and finite element methods to characterise the machine have not yielded conclusive results. Without experimental data, it is difficult to ascertain which method is a more accurate depiction of the machine – although it is likely to be the more sophisticated FEA model. As a result of this, data will be collected from the Durham University Solar Car during its race to then compare with the data obtained so far.

While unfortunate, it has been shown that a Halbach array would not be beneficial for the current edition of the DUSC solar car without serious redesign of the stator windings. This could perhaps be worked on in a future project.

Finally, new sculpted back irons were machined for the current DUSC motor, *Eadfrith*, and are shown in Figures 12 and 13.

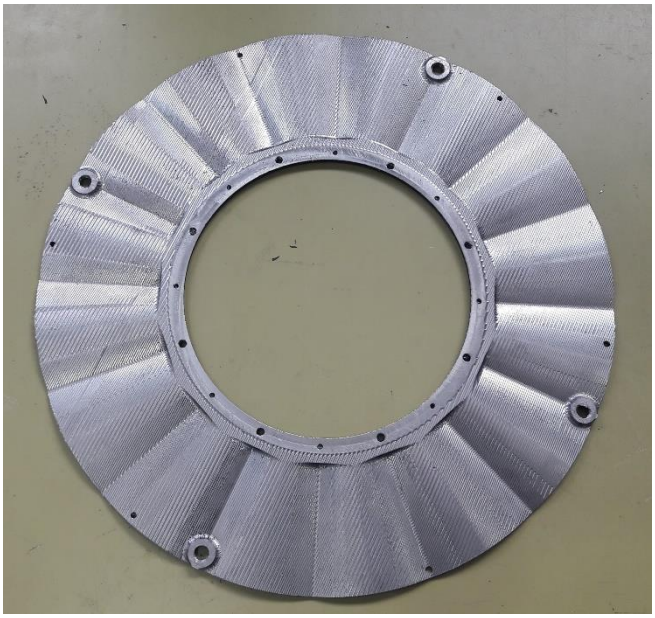

Figure 11: Completed LHS back-iron

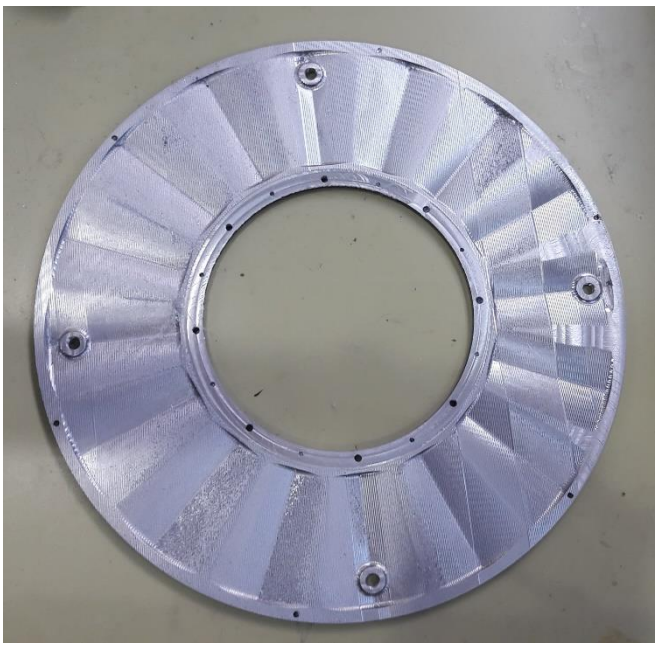

Figure 12: Completed RHS back-iron

These back-irons have ended up weighing slightly more than initial calculations predicted, coming in at just under 3.5kg each. This still grants an overall weight gain of 3kg which will ultimately help the Durham Solar Car in the Bridgestone World Solar Challenge.

V. References

[1] J.R. Bumby, R. Martin, M.A Mueller, E. Spooner, N.L. Brown, B.J Chalmers (2004). *'Electromagnetic design of axial-flux permanent magnet machines'* Durham University Department of Engineering.

[2] J. F. Gieras, R Wang, M. J. Kamper (2008). *'Axial Flux Permanent Magnet Brushless Machines'* (2nd Edition, Pg. 45-53).

[3] O. Winter, C. Kral, E. Schmidt (2012). *'Design study of magnet shapes for axial Halbach arrays using 3D finite element analyses'* 2012 XXth International Conference on Electrical Machines.

[4] U. Javed, C Donaghy-Spargo (2017). *'Design Improvements in an Axial Flux Machine for a Solar Electric Vehicle'* Durham University Department of Engineering.

[55] J. Brown (2010). *'High Efficiency Permanent Magnet Motor'* Marand Precision Engineering.

[6] A. Hughes (1990). *'Electric Motors and Drives'* (2nd Edition, Pg. 13-14).